INTERNATIONAL JOURNAL FOR NUMERICAL METHODS IN FLUIDS
Int. J. Numer. Meth. Fluids 2004; **44**:721–735 (DOI: 10.1002/fld.661)

Finite element solution of the Orr–Sommerfeld equation using high precision Hermite elements: plane Poiseuille flow

M. Mamou*,† and M. Khalid

Institute for Aerospace Research, National Research Council Canada, Ottawa, Ontario, Canada K1A 0R6

SUMMARY

This paper presents a comprehensive review of the numerical techniques used during the past half century and their accuracy in hydrodynamic stability analysis of plane parallel flows. The paper also describes a finite element solution of the Orr–Sommerfeld equation using high precision Hermite elements. A stability analysis technique is performed by imposing an infinitesimal perturbation to the laminar base flow to determine the thresholds of neutral instabilities or the growth rate of the perturbation for any Reynolds and wave numbers. Validation of the present numerical technique is performed for plane Poiseuille flow. The numerical results, obtained with uniform and nonuniform meshes, show excellent agreement with the most accurate results available in the literature. Copyright © 2004 John Wiley & Sons, Ltd.

KEY WORDS: finite element; Orr–Sommerfeld equation; eigenvalue problem; quintic hermite elements

1. INTRODUCTION

A true understanding of transition flows has eluded aerodynamicists for decades. Since turbulence and chaos pervade across all flow regimes, the character of transition-evoking instabilities must be understood in all types of flows including subsonic, transonic, supersonic, and hypersonic. The fundamental nature of instabilities is similar in most flows. Therefore, aerodynamicists have concentrated on classic low Reynolds number flows at low speeds which can be analyzed with a certain degree of confidence using controlled experiments. Once a satisfactory theoretical model that describes the onset of instabilities in the laminar flow regime of low Reynolds number subsonic flows has evolved and been validated, one may envisage its extension to other flow regimes.

Accurate prediction of the onset of instabilities in laminar flows by solving the Orr–Sommerfeld equation using discrete numerical methods has been a true challenge. Despite the available computer resources, with increased speed and memory storage space, discrete

*Correspondence to: M. Mamou, Institute for Aerospace Research, National Research Council Canada, Montreal Road, Building U66 Uplonds, Ottawa, Ontario, K1A 0R6, Canada.
†E-mail: mahmoud.mamou@nrc-cnrc.gc.ca

Received 3 March 2003
Revised 8 September 2003

numerical techniques such as the finite difference and finite element methods, which use a limited number of grid points or finite elements, have not been able to predict the critical Reynolds number and the wave number with a high degree of accuracy. An accurate discrete solution to the Orr–Sommerfeld equation requires efficient discretization tools. The critical Reynolds number for the onset of instability is relatively high for many classical laminar flows; hence, the shear flows effects are confined to a thin layer near the flow boundaries, and are characterized by steep gradients of the flow properties, in the close vicinity of the boundaries. In the bulk region of the flow where the viscous effects and vorticity production are weak, the flow property gradients are usually relatively small. Therefore, clustering and stretching over these regions are natural ways to obtain a solution with fewer grid points and sufficient accuracy. The accuracy itself is dependent upon the numerical technique employed. For the same number of grid points/elements and distribution, for example, a finite element method can perform much better than a finite difference method even with high order schemes.

A numerical solution of the Orr–Sommerfeld equation leads to a set of eigenvalues for the perturbation growth rate called spectrum-containing a finite number of different modes. The number and the precision of the modes will depend eventually on the grid size of the numerical domain. In other words, the number of modes will be equal to the degrees of freedom within the numerical domain. Finding the most instable (or least stable) mode is straightforward using a local iterative procedure with a very good guess for the initial values. This technique is less cost effective; however, there is a great risk of missing the least stable mode or the most dangerous mode. To avoid this risk, it is more convenient to use a global iterative procedure that will determine all the spectra (possible decaying and growing modes) and identify the most instable (or the least stable) modes. A global technique, which is adopted in the present study, is more costly than a local technique but it is completely reliable.

For an undisturbed plane Poiseuille flow, the basic solution is given in dimensionless form as

$$U_b = 1 - y^2 \tag{1}$$

The half width, h', between the two parallel planes and the velocity at the mid-width of the channel, U_0, are used for scaling such that the flow domain is given by $\Omega = \{y \in [-1, 1]\}$ and the Reynolds number is given by $Re = U_0 h'/\nu$, where ν is the kinematic viscosity of the fluid.

Following the notation of Orszag [1], a two-dimensional disturbance is described by

$$V(t, x, y) = v(y) e^{i\alpha(x - \lambda t)} \tag{2}$$

where V is the y-perturbation-velocity component, $\sigma = -i\alpha\lambda$ is the growth rate of the perturbation, and α is the wave number in the flow direction.

The Orr–Sommerfeld equation is obtained as follows:

$$\frac{\partial^4 v}{\partial y^4} - 2\alpha^2 \frac{\partial^2 v}{\partial y^2} + \alpha^4 v - i\alpha Re \left[(U_b - \lambda) \left(\frac{\partial^2 v}{\partial y^2} - \alpha^2 v \right) - \frac{\partial^2 U_b}{\partial y^2} v \right] = 0 \tag{3}$$

and the boundary conditions are

$$y = \pm 1, \quad v = \frac{\partial v}{\partial y} = 0 \tag{4}$$

Table I. Critical parameters at the onset of instabilities for plane Poiseuille flow. The superscripts h' and $h'/2$ refer to computations within full and half channel flow configurations.

References	Re_c	α	λ_r
Thomas [11]	5780	1.026	—
Grosch and Salwen [4]	5750	1.025	—
Orszag [8]	5772.22	1.02056	0.26400174
Saraph *et al.* [9]	$5882^{h'}$, $5848^{h'/2}$	—	—
Kirchner [5]	5775.99	1.026	—

Table II. Perturbation growth rate for $Re = 10^4$ and $\alpha = 1$ for plane Poiseuille flow.

References	λ_r	λ_i
Thomas [11]	0.2375259	0.0037404
Grosch and Salwen [4]	0.237413	0.003681
Orszag [8]	0.23752649	0.00373967
Dongarra *et al.* [1]	0.23752708	0.00373980
Kirchner [5]	0.23752648882047	0.003739670622979582

During the last half century, many researchers have presented different numerical techniques for solving the Orr–Sommerfeld equation for plane Poiseuille flow. The most used numerical techniques are finite difference, spectral, and finite element methods. Most of the previous work has considered the special case of $Re = 10^4$ and $\alpha = 1$, and the case of the onset of neutral instability. Some previous results are listed in Tables I and II for comparison.

A literature review demonstrates that the number of studies concerning this particular problem is vast. Therefore, only those most relevant have been referenced in this paper. Starting with the early work of Thomas [2], the Orr–Sommerfeld equation was solved using fourth-order finite difference scheme with a uniform mesh. The number of grid points was varied between 50 and 100. The results were obtained by extrapolating to a zero grid spacing. The author also presented results in terms of the perturbation growth rate for different values of Re and α.

Grosch and Salwen [3, 4] solved the Orr–Sommerfeld equation in terms of a stream function formulation. The perturbation stream function was expanded in a truncated series of functions that satisfied the boundary conditions. A Galerkin method was employed to solve the Orr–Sommerfeld equation, and the QR algorithm was used to solve the resulting eigenvalue problem for a given Re and α. Results in terms of the growth rate were presented for different values of Re and α.

A more accurate solution of the Orr–Sommerfeld equation for plane Poiseuille flow was obtained by Orszag [1]. Reducing the perturbed Navier–Stokes equations, the author used a pseudo-spectral method by expanding the flow variable into Chebyshev polynomials. The resulting eigenvalue problem was solved using the QR matrix eigenvalue algorithm. The most accurate results were obtained using up to 50 Chebyshev polynomials and different round-off errors, as displayed in Tables I and II.

Saraph *et al.* [5] used a finite element method to solve the Orr–Sommerfeld equation. The authors applied the Galerkin technique with linear weighting functions for the continuity

equation and quadratic weighting functions for the momentum equation. The results were presented for full and half channel flow in terms of the critical Reynolds number for the onset of instability. Due to the low number of finite elements used in both configurations (four elements) the results were not accurate as those of Orszag [1] (see Table I).

Mele *et al.* [12] solved the Orr–Sommerfeld equation by a finite element method, using Hermite cubic elements with non-uniform mesh. The results were obtained for $\alpha = 1$ and $Re = 10^4$ (see Table II). The eigenvalues are obtained by solving the resulting matrix system by the QR algorithm. The number of elements was varied from 15 to 43. A good accuracy was obtained with 43 elements on a half channel when accounting for symmetry. Fortin *et al*. [6] developed a practical and accurate numerical method, based on a finite element method, to solve the Orr–Sommerfeld equation for Poiseuille flow. They also determined the threshold for finite amplitude instabilities (known as subcritical flow). The algorithm of their numerical technique is described in detail in Reference [6]. The Q2-P1 element (quadratic for velocity component and linear for pressure) is used. Their results were obtained in terms of the growth rate at the threshold of instability that was determined previously by Orszag [1]. On a refined mesh, the value of the growth rate agreed to six digits with Orszag's results.

Dongarra *et al*. [7] used Chebyshev tau-QZ algorithm methods to compute the spectra of classical laminar flows. In their methods, the authors used Chebyshev representations of the fourth derivative operator (D^4 method). For plane Poiseuille flow with $Re = 10^4$ and $\alpha = 1$, the authors claimed to have obtained the best results using the D^4 method with 50 polynomials. They claimed these results were at least as good as or better than the results reported by Orszag [1]. They also reported that the method diverged when the number of polynomials was increased above 50.

Recently, Kirchner [8] introduced a spectral Galerkin finite element method (p-FEM method) to solve the Orr–Sommerfeld equation. The eigenfunction was developed into a truncated series of shape functions consisting of the Legendre polynomials. The numerical domain mesh contained only one finite element; the accuracy improvement was obtained by increasing the polynomial degree instead of improving the mesh refinement. A polynomial degree of 100–500 was used and the results agreed well with those reported by Orszag [1]. However, the results at the onset of instability were not as accurate as Orszag's results. Their analysis indicated that the p-FEM method used was similar to a spectral method, since the boundary conditions were applied to the shape functions rather than to the shape function coefficients, which is the usual implementation in a finite element method.

The previous studies have proved the capabilities of the Galerkin and spectral methods in obtaining accurate results when solving the Orr–Sommerfeld equation. However, for discrete techniques such as finite difference and finite element methods, the results are not as accurate as those obtained using the methods discussed above. This is probably due to inappropriate choices of the grid distribution strategy and to the discretization schemes. High order schemes or high precision finite elements are required due to the steep flow properties's gradients near the boundaries. Also, appropriate clustering and stretching of the grid points within the numerical domain may help obtain results with a high degree of accuracy.

In the present paper, a finite element method with high precision elements is used to solve the Orr–Sommerfeld equation. The finite element procedure is described in Section 2. The results and a discussion are presented in Section 3, and some concluding remarks are given in Section 4.

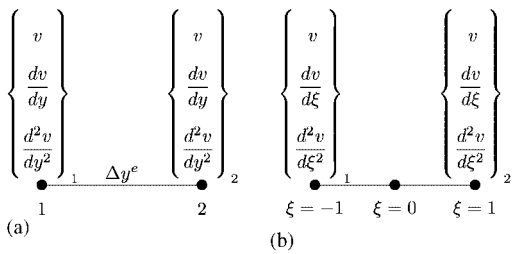

Figure 1. Quintic hermite element: (a) finite element; (b) master element.

2. NUMERICAL FORMULATION

The Orr–Sommerfeld equation is solved using the Bubnov–Galerkin technique. High precision Hermite elements are used to discretize the Galerkin integral form of the Orr–Sommerfeld equation.

2.1. Variational formulation

The Galerkin or the variational formulation is a weighted residual technique that uses for a weighting function any test function ϕ that satisfies $\phi \in H_0^2(\Omega)$, with $H_0^2(\Omega) = \{\phi \in H^2(\Omega)/\ \phi = \partial\phi/\partial y = 0 \text{ on } \Gamma\}$, and $H^2(\Omega)$ is the Sobolev space of square integrable functions including their first and second derivatives, and $\Gamma = \partial\Omega$ is the domain boundary. Multiplying the Orr–Sommerfeld equation by ϕ, and making use of the Green theorem, and then integrating over the physical domain Ω leads to the following formulation:

$$\int_\Omega \frac{\partial^2 v}{\partial y^2}\frac{\partial^2 \phi}{\partial y^2}\,\mathrm{d}y + \left[\frac{\partial^3 v}{\partial y^3}\phi\right]_{y=-1}^{y=1} - \left[\frac{\partial^2 v}{\partial y^2}\frac{\partial \phi}{\partial y}\right]_{y=-1}^{y=1}$$
$$+ \int_\Omega 2\alpha^2 \frac{\partial v}{\partial y}\frac{\partial \phi}{\partial y}\,\mathrm{d}y - 2\alpha^2\left[\frac{\partial v}{\partial y}\phi\right]_{y=-1}^{y=1} + \int_\Omega \alpha^4 v\phi\,\mathrm{d}y$$
$$+ \int_\Omega \left[\mathrm{i}\alpha R_e U_b\left(\frac{\partial^2 v}{\partial y^2} - \alpha^2 v\right)\phi + \mathrm{i}\alpha R_e \frac{\partial^2 U_b}{\partial y^2} v\phi\right]\mathrm{d}y$$
$$= \mathrm{i}\alpha R_e \lambda \int_\Omega \left(\frac{\partial v}{\partial y}\frac{\partial \phi}{\partial y} + \alpha^2 v\phi\right)\mathrm{d}y - \mathrm{i}\alpha R_e \lambda\left[\frac{\partial v}{\partial y}\phi\right]_{y=-1}^{y=1} \tag{5}$$

Since $\phi \in H_0^2(\Omega)$, the boundary integral, known as the natural boundary conditions, vanish.

Equations (5) were discretized using the finite element method. The Hermite element was used to satisfy the essential and the natural boundary conditions (4) (see Figure 1). The Hermite elements are usually used to guarantee a C^1 continuity across the element faces. In other words, this type of element provides inter-element continuity of the flow field variables at the nodal points. For high order partial differential equations, it is recommended to use such type of elements which allows the satisfaction of all the boundary conditions. At each node of the element, the functional representation for any flow field variable must include more degrees

of freedom than the nodal value. The additional degrees of freedom are usually represented by the first, second, etc., derivatives of the variables, which are regarded as unknowns. In the presented study a cubic and quintic Hermite element is used to solve the Orr–Sommerfeld equation. For a cubic element the number of degrees of freedom is two; the flow field variable its self (v) and its first derivative ($\mathrm{d}v/\mathrm{d}y$). For a quintic element, there is an additional degree of freedom which is represented by the second derivative of the flow field variable ($\mathrm{d}^2v/\mathrm{d}y^2$), see Figure 1. Thus, in each element, the velocity component profile is given by

$$\begin{aligned} v(y)&=\sum_{j=1}^{2}\left[v_j\mathscr{H}_j(\xi)+\frac{\partial v_j}{\partial y}\,\mathscr{H}_{j+2}(\xi)\right] \quad \text{for cubic element}\\ v(y)&=\sum_{j=1}^{2}\left[v_j\mathscr{H}_j(\xi)+\frac{\partial v_j}{\partial y}\,\mathscr{H}_{j+2}(\xi)+\frac{\partial^2 v_j}{\partial y^2}\,\mathscr{H}_{j+4}(\xi)\right] \quad \text{for quintic element} \end{aligned} \tag{6}$$

where $\mathscr{H}$ are the Hermite interpolation functions. The parameter ξ refers to the master element co-ordinate such that $y=\xi\Delta y^e/2$. The variable v is a complex function and $\mathscr{H}$ is a real function. Therefore, the coefficients (nodal values) v_j, $\partial v_j/\partial\xi$ and $\partial^2 v_j/\partial\xi^2$ are the unknown complex numbers.

The Hermite shape functions are defined as follows:

$$\begin{aligned} &v:\mathscr{H}_i(\xi)=(\xi+\xi_i)^2(\xi\xi_i-2)\,\tfrac{1}{4}\\ &\frac{\partial v}{\partial\xi}:\mathscr{H}_{i+2}(\xi)=-\xi_i(\xi+\xi_i)^2(\xi\xi_i-1)\frac{\mathscr{J}}{4}, \quad i=1,2 \text{ for cubic element}\\ &v:\mathscr{H}_i(\xi)=(1+\xi_i\xi)^3(8-9\xi_i\xi+3\xi^2)\,\tfrac{1}{16}\\ &\frac{\partial v}{\partial\xi}:\mathscr{H}_{i+2}(\xi)=(1+\xi_i\xi)^3(-\xi_i+\xi)(5-3\xi_i\xi)\frac{\mathscr{J}}{16}, \quad i=1,2 \text{ for quintic element}\\ &\frac{\partial^2 v}{\partial\xi^2}:\mathscr{H}_{i+4}(\xi)=(1+\xi_i\xi)^3(1-\xi_i\xi)^2\,\frac{\mathscr{J}^2}{16} \end{aligned}$$

Here $\xi_1=-1$, $\xi_2=1$ and $\mathscr{J}=\Delta y^e/2$ is the Jacobian, where Δy^e is the element size.

2.2. Finite element formulation

Following the Bubnov–Galerkin procedure, after assembling to a global system, the elementary integral form of the Orr–Sommerfeld equation (5), was obtained as follows:

$$[A]\{v\}=\lambda[B]\{v\} \tag{7}$$

where $[A]$ and $[B]$ are square matrices of dimension $M\times M$. The parameter M represents the total degrees of freedom within the discretized domain $M=l\times(N+1)$, where N is the number of the finite elements used in y-direction and l is related to the precision of the Hermite element ($l=2$ for cubic elements and 3 for quintic elements). The elementary matrices are:

$$[A]=\int_{\Delta y^e}\left[\frac{\partial^2\mathscr{H}_i}{\partial y^2}\,\frac{\partial^2\mathscr{H}_j}{\partial y^2}+2\alpha^2\,\frac{\partial\mathscr{H}_j}{\partial y}\,\frac{\partial\mathscr{H}_i}{\partial y}+\alpha^4\mathscr{H}_j\mathscr{H}_i\right.$$

$$+\mathrm{i}\alpha R_e U_b \left(\frac{\partial^2 \mathscr{H}_j}{\partial y^2} - \alpha^2 \mathscr{H}_j\right) \mathscr{H}_i + \mathrm{i}\alpha R_e \frac{\partial^2 U_b}{\partial y^2} \mathscr{H}_j \mathscr{H}_i \Bigg] \, \mathrm{d}y$$

$$[B] = -\mathrm{i}\alpha R_e \int_{\Delta y^e} \left(\frac{\partial \mathscr{H}_j}{\partial y} \frac{\partial \mathscr{H}_i}{\partial y} + \alpha^2 \mathscr{H}_j \mathscr{H}_j\right) \mathrm{d}y \tag{8}$$

To avoid numerical integration errors, the above integrals are accurately computed using eight points of Gauss.

2.3. Boundary conditions

The boundary conditions in Equation (4) are introduced without altering the dimensions of the matrices $[A]$ and $[B]$. From Equation (4), one can deduce that:

$$\begin{aligned} v_1 &= \frac{\partial v_1}{\partial y} = 0 \\ v_{N+1} &= \frac{\partial v_{N+1}}{\partial y} = 0 \end{aligned} \tag{9}$$

where 1 refers to the first node of the first element and $N+1$ refers to the last node of the last element N. For the unknown variable v_j at the first node of the first element (i.e. at $y=-1$), the boundary conditions are introduced in Equation (7) as follows:

$$\begin{aligned} &[A]_{1,j} = [A]_{i,1} = [B]_{1,j} = 0 \quad \text{for all } i \text{ and } j \\ &[A]_{1,1} = \beta, \quad [B]_{1,1} = -\mathrm{i}\beta \end{aligned} \tag{10}$$

where β is a real number which could be set to any positive value, such that the spurious eigenvalues are given by $\lambda = 0 - \mathrm{i}\beta$. It is recommended to consider large value of β (i.e. $\beta = 10^6$) such that the spurious eigenvalues correspond to the most stable modes. Similar technique is applied for the other boundary conditions (i.e. at $y=1$).

2.4. Threshold for oscillatory flows

The transition from steady to oscillatory laminar flows indicates the early stage of transition to turbulence. A linear stability analysis determines the threshold, Re_C, above which instabilities develop. Above the threshold, the perturbations may grow with time in a monotonic or an oscillatory manner. The perturbation growth rate is related to λ ($\lambda = \lambda_r + \mathrm{i}\lambda_i$). For a given wave number α, the eigenvalue λ and eigenfunctions $\{v\}$ are computed for different Reynolds numbers and wave numbers. The solution of the eigenvalue problems leads to M eigenvalues λ_i, with $i = 1, 2, \ldots, M$. The onset of instabilities is obtained by observing when the imaginary part of λ changes from negative to positive values in only one eigenvalue. If the real part of the eigenvalue is not zero, then the instability is oscillatory. In this manner, the critical Reynolds number can be obtained for different wave numbers. The minimum Reynolds number for all wave numbers represents the threshold of instabilities, and the corresponding wave number is the critical one.

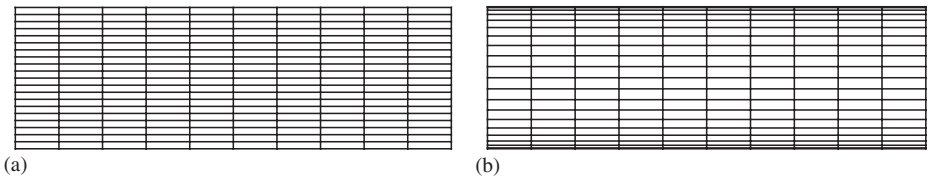

Figure 2. (a) Uniform grid, (b) non-uniform grid: sinusoidal distribution.

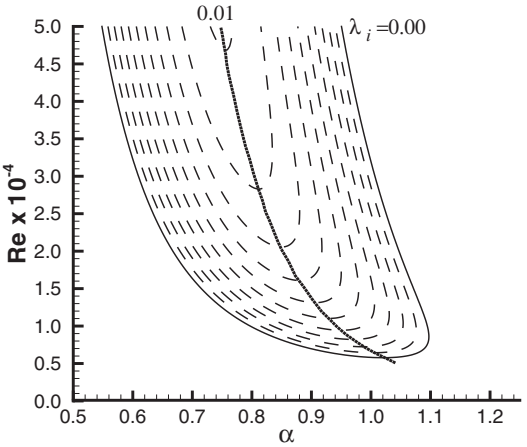

Figure 3. Stability diagram for plane Poiseuille flow obtained with 60 quintic hermite elements.

3. RESULTS AND DISCUSSION

All of the results presented in the present paper were obtained using double precision variables. Due to the boundary conditions constraints, the high gradient velocities were confined to a small layer near the horizontal planes. Two meshes were considered to study the grid sensitivity. The first mesh was uniform. The second mesh used a sinusoidal distribution such that the grid was more refined near the boundaries (see Figure 2(a) and (b)). The sinusoidal grid distribution is given in terms of the finite element size defined as follows:

$$\Delta Y_{ej} = \left| \sin\left(\frac{\pi}{2} + \frac{(j-1)\pi}{N}\right) - \sin\left(\frac{\pi}{2} + \frac{j\pi}{N}\right) \right|, \quad j = 1, N \tag{11}$$

The eigenvalue problem described by Equation (7) was solved using the double precision subroutine DGVCCG from the IMSL library.

Figure 3 shows the stability diagram for the *Re*–α plane. The outer curve gives the boundary for the onset of the neutral instability; this corresponds to $\lambda_i = 0$. All of the contours correspond to constant λ_i. For any Reynolds number, a vertical curve indicates the maximum growth rate of the perturbations and the corresponding wave number.

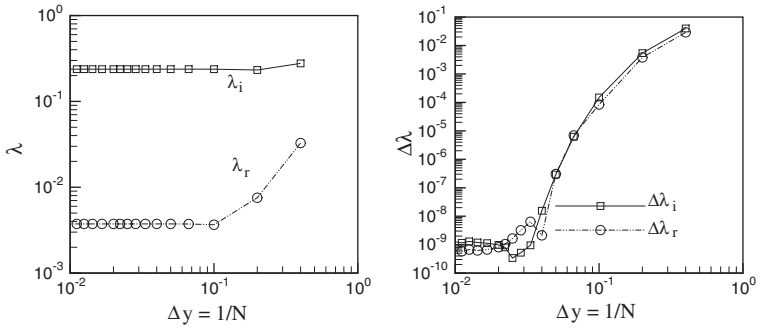

Figure 4. Grid size effect on the computed growth rate and pulsation of the perturbation for $Re = 10^4$ and $\alpha = 1$ using quintic hermite elements. $\Delta\lambda_e$ represents the difference between the present computed values and Orszag's results.

Table III. Grid size effect on the computed critical Reynolds and wave numbers at the onset of oscillatory flows using quintic hermite element with uniform and sinusoidal meshes.

N	α_c	$\Delta\alpha_c$	Re_c	ΔRe_c	λ_r	λ_i	$\lvert\Delta\lambda_r\rvert$
Uniform mesh							
10	1.0276203	7.060E − 03	5469.1997	3.03E + 02	0.26486483	8.3E − 15	8.63E − 03
20	1.0198174	7.426E − 04	5782.8900	1.07E + 01	0.26378104	2.4E − 14	2.21E − 03
30	1.0205113	4.875E − 05	5772.8572	6.37E − 1	0.26398959	3.7E − 14	1.22E − 04
40	1.0205461	1.389E − 05	5772.2364	1.64E − 02	0.26399991	6.7E − 13	1.83E − 05
50	1.0205502	9.805E − 06	5772.2196	3.60E − 04	0.26400059	3.3E − 13	1.15E − 05
Sinusoidal mesh							
10	1.0179694	2.591E − 03	5831.9731	5.98E + 01	0.26315593	8.72E − 15	8.46E − 04
20	1.0205948	3.479E − 05	5770.7306	1.49E + 00	0.26401834	4.80E − 14	1.66E − 05
30	1.0205477	1.227E − 05	5772.2066	1.34E − 02	0.26400036	1.91E − 13	1.38E − 06
40	1.0205429	1.715E − 05	5772.2218	1.78E − 03	0.26399972	2.92E − 12	2.02E − 06
50	1.0205315	2.851E − 05	5772.2216	1.59E − 03	0.26399840	2.74E − 12	3.34E − 06

The results obtained for $\alpha = 1$ and $Re = 10^4$ were compared to Orszag's results [1]. Figure 4 illustrates the effect of the grid size on the computed values. As can be seen from Figure 4(b), the present results converge to those reported by Orszag [1] within a difference of about 10^{-9}. Table III lists the grid size effects on the computed critical parameters at the onset of instabilities. These results are compared to those of Orszag [1], which are denoted in Equation (12) by the subscript a (i.e. accurate):

$$\begin{aligned} \Delta\alpha_C &= |\alpha_C - \alpha_{C\mathrm{a}}| \\ \Delta Re_C &= |Re_C - R_{C\mathrm{a}}| \\ \Delta\lambda_r &= \mathrm{Real}(\lambda - \lambda_{\mathrm{a}}) \\ \Delta\lambda_i &= \mathrm{Imag}(\lambda - \lambda_{\mathrm{a}}) \end{aligned} \tag{12}$$

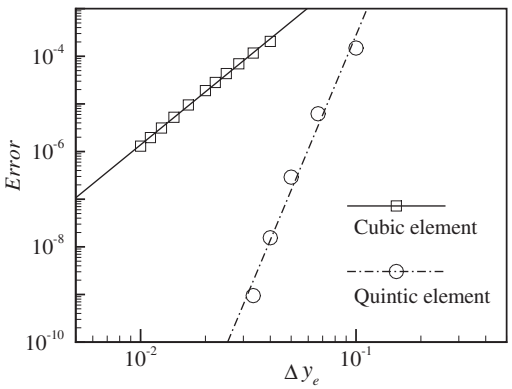

Figure 5. Convergence rate for the most stable mode with $\alpha = 1$ and $Re = 10^4$, using uniform grid.

where $\alpha_{Ca} = 1.02056$, $R_{Ca} = 5777.22$, and $\lambda_a = 0.26400174 + i0$ for the onset of instabilities. For $Re = 10000$ and $\alpha = 1$, $\lambda_a = 0.23752649 + i0.00373967$ [1].

The error estimation for the perturbation flow field (v) is given by the following usual expression:

$$|v - v_{\Delta y_e}|_n \leqslant C \Delta y_e^{k+1-n} \tag{13}$$

where C is a positive constant, the parameter k is related to the polynomial order of the shape functions and n to the Sobolev space ($H_0^n(\Omega)$ with $n = 2$ for the present problem). Therefore, the convergence rate ($k + 1 - n$) is of order two for cubic Hermite element ($k = 3$) and four for quintic element ($k = 5$).

A convergence analysis for the computed eigenvalues is presented for the most unstable mode with $\alpha = 1$ and $Re = 10^4$. Using cubic and quintic elements, the error is given by

$$\text{Error} = |\text{Real}(\lambda - \lambda_a)| = C \Delta y_e^r \tag{14}$$

is displayed in Figure 5 as a function of the finite element size; Δy_e, using uniform grid distribution. The computed values are presented in the figure by symbols. A power fitting curve ($\text{Error} = C \Delta y_e^r$, shown in the figure with straight lines) is performed for each case and the estimated error expression is obtained as follows:

$$\begin{aligned} &\text{Error} = 34.2 \Delta y_e^{3.7} \quad \text{for cubic element} \\ &\text{Error} = 1.8 \times 10^7 \Delta y_e^{10.8} \quad \text{for quintic element} \end{aligned} \tag{15}$$

At the first glance, the quintic high precision Hermite element displays a very high convergence rate, but its constant is very large. Nevertheless, the error dives to zero more rapidly than the cubic Hermite element case. Thus, a best accuracy could be obtained with only a few quintic elements.

Table IV. Uniform grid size effects on the computed value of λ for $Re = 10\,000$ and $\alpha = 1$, using a quintic hermite element.

N	λ_r	λ_i	$\lvert\Delta\lambda_r\rvert$	$\lvert\Delta\lambda_i\rvert$
5	0.2773423866	0.03273227546	3.9816E − 02	2.8992E − 02
10	0.2321009532	0.00754796418	5.4255E − 03	3.8083E − 03
20	0.2373776055	0.00365547838	1.4888E − 04	8.4192E − 05
30	0.2375202777	0.00373278188	6.2123E − 06	6.8881E − 06
40	0.2375261993	0.00373936516	2.9068E − 07	3.0484E − 07
50	0.2375264745	0.00373966788	1.5520E − 08	2.1212E − 09
60	0.2375264909	0.00373967637	9.4714E − 10	6.3866E − 09
70	0.2375264905	0.00373967320	5.2108E − 10	3.2006E − 09
80	0.2375264897	0.00373967164	3.3878E − 10	1.6449E − 09
90	0.2375264892	0.00373967104	8.0072E − 10	1.0434E − 09
100	0.2375264890	0.00373967081	9.7820E − 10	8.1093E − 10
120	0.2375264889	0.00373967067	1.1241E − 09	6.7173E − 10
140	0.2375264888	0.00373967062	1.1885E − 09	6.2317E − 10
160	0.2375264887	0.00373967067	1.3010E − 09	6.6817E − 10
180	0.2375264888	0.00373967058	1.1550E − 09	5.8455E − 10
200	0.2375264887	0.00373967061	1.2565E − 09	6.1064E − 10
Orszag [8]	0.23752649	0.00373967	—	—
Kirchner [5]	0.23752648882047	0.00373967062297958 2	—	—

Table V. Non-uniform grid size effects on the computed value of λ for $Re = 10\,000$ and $\alpha = 1$, using a quintic hermite element.

N	λ_r	λ_i	$\lvert\Delta\lambda_r\rvert$	$\lvert\Delta\lambda_i\rvert$
5	0.2313468705	0.00589349592	6.1796E − 03	2.1538E − 03
10	0.2372547840	0.00397284684	2.7171E − 04	2.3318E − 04
20	0.2375277348	0.00373666575	1.2448E − 06	3.0043E − 06
30	0.2375265808	0.00373955990	9.0796E − 08	1.1010E − 07
40	0.2375264877	0.00373967121	2.2588E − 09	1.2082E − 09
50	0.2375264874	0.00373967223	2.6315E − 09	2.2338E − 09
60	0.2375264886	0.00373967084	1.3938E − 09	8.4357E − 10
70	0.2375264571	0.00373970564	3.2946E − 08	3.5638E − 08
80	0.2375264930	0.00373967037	3.0296E − 09	3.7256E − 10
100	0.2375264694	0.00373965259	2.0580E − 08	1.7410E − 08
120	0.2375264386	0.00373960991	5.1389E − 08	6.0090E − 08
140	0.2375266268	0.00374005593	1.3683E − 07	3.8593E − 07
160	0.2375264269	0.00373982898	6.3098E − 08	1.5898E − 07
180	0.2375268635	0.00373768946	3.7353E − 07	1.9805E − 06
200	0.2375261430	0.00373667921	3.4697E − 07	2.9908E − 07

The results, for different grid sizes, are given in Tables III for the onset of instabilities and in Tables IV and V for $\alpha = 1$ and $Re = 10^4$. The computed results converge towards the accurate values, reported by Orszag [1], as the number of elements is progressively increased.

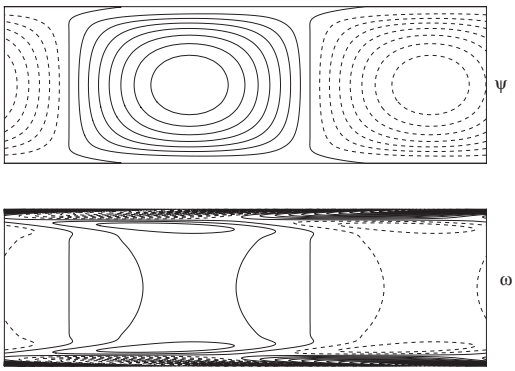

Figure 6. Perturbation flow and vorticity patterns at the onset of oscillatory flows.

The results also indicate that the accuracy of the non-uniform grid is much better than that of the uniform grid, for the same number of elements. With the non-uniform grid, the accuracy is excellent with 40 finite elements. It is noticed that when the number of element increases beyond 40, the solution became less accurate. This is due to the fact that when the number of element is increased the size of the first element near the walls became very small. Therefore, the finite element integration over these elements leads to very small values when compared to the other elements values (i.e. for $N = 200$, the maximum and the minimum values of the matrix $[A]$ are obtained as $(9130209049753.91 + \mathrm{i}24283.5166742748)$ and $(1.762393122114774 \times 10^{-6} + \mathrm{i}9.191382668079178 \times 10^{-16})$, respectively. Hence, to capture well the accuracy, the numerical code has to be switched from double to high precision variables.

To illustrate the secondary flows generated by the growing perturbation, a stream function Ψ is defined as follows:

$$W = -\frac{\partial \Psi}{\partial x} \quad \text{and} \quad U = \frac{\partial \Psi}{\partial y} \tag{16}$$

such that the continuity equation is automatically satisfied. The perturbation for the stream function ψ is

$$\psi = \frac{-\mathrm{i}}{\alpha} \mathrm{e}^{\mathrm{i}\alpha(x-\lambda t)} v \tag{17}$$

and the vorticity field is

$$\omega = -\nabla^2 \psi = \frac{-\mathrm{i}}{\alpha} \mathrm{e}^{\mathrm{i}\alpha(x-\lambda t)} \left(-\alpha^2 v + \frac{\mathrm{d}^2 v}{\mathrm{d}\, y^2} \right) \tag{18}$$

The perturbation stream function and vorticity contours at the onset of instabilities are illustrated in Figure 6. The perturbation vorticity gradient is enhanced near the top and bottom boundaries.

The vertical velocity of the perturbation and its derivatives are shown in Figure 7. It is clear that the derivative functions exhibit steep gradients near the boundaries. Thus it is important

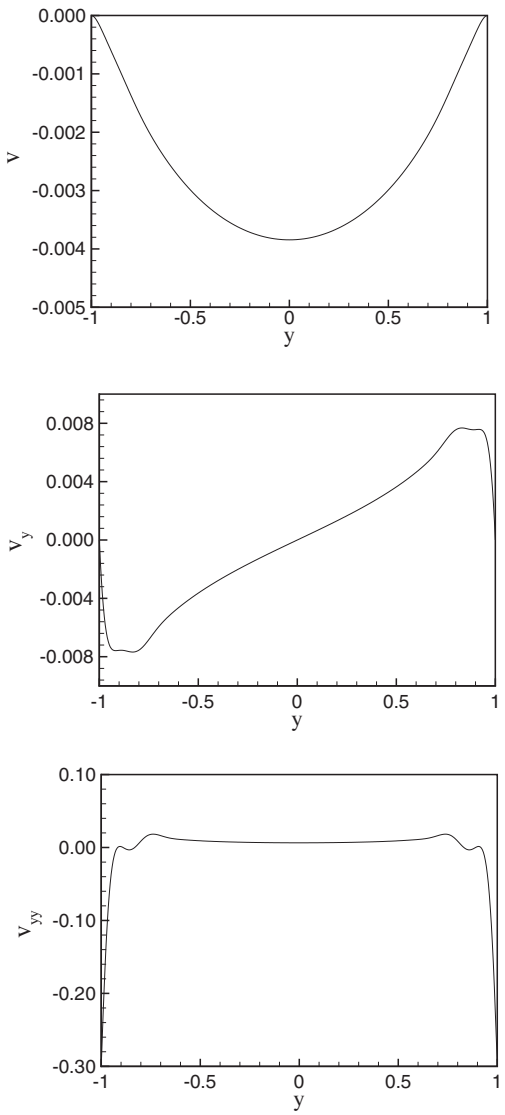

Figure 7. Vertical velocity of the perturbation and its derivatives.

to use a non-uniform grid to capture the flow details using as few finite elements as possible. Finally, the effect of finite element order is studied. The results listed in Table VI for $Re = 10^4$ and $\alpha = 1$ show that increasing the order of the Hermite element considerably increases the accuracy of the results. When using 60 quintic elements, with non-uniform mesh, the results agreed to nine digits with the accurate results reported by Kirchner [8]. Further increases in the element number gave less precision, as the first element size near the wall became very small.

Table VI. Comparison between cubic and quintic hermite element results for non-uniform grid with $Re = 10\,000$ and $\alpha = 1$.

N	λ_r	λ_i
(a) *Cubic element*		
10	0.2406497285	0.0075862465
20	0.2381202250	0.0042009069
30	0.2375665423	0.0038182006
40	0.2375310856	0.0037651408
50	0.2375281310	0.0037501097
60	0.2375272276	0.0037447320
70	0.2375268699	0.0037424113
80	0.2375267058	0.0037412803
90	0.2375266211	0.0037406770
100	0.2375265740	0.0037403318
200	0.2375264951	0.0037397010
[5]	0.2375264888	0.0037396706
(b) *Quintic element*		
10	0.2372547840	0.0039728468
20	0.2375277348	0.0037366657
30	0.2375265808	0.0037395599
40	0.2375264877	0.0037396712
50	0.2375264874	0.0037396722
60	0.2375264886	0.0037396708
70	0.2375264571	0.0037397056
80	0.2375264930	0.0037396704
90	0.2375264862	0.0037396538
100	0.2375264694	0.0037396526
200	0.2375261430	0.0037366792
[5]	0.2375264888	0.0037396706

4. CONCLUSION

A numerical linear stability analysis of developed laminar flows was used to determine the critical Reynolds number above which a steady laminar flow becomes unstable to infinitesimal perturbations. A finite element method was proposed to solve the Orr–Sommerfeld equation, using high precision Hermite finite elements. The results were presented for cubic and quintic Hermite elements and with uniform and non-uniform grid distributions. The results showed an excellent agreement with the most accurate results available in the literature. A best accuracy is obtained with few elements (40 elements) using a non-uniform grid (sinusoidal distribution) and a quintic high precision Hermite element. For uniform grid distribution, it was found that the convergence rate of the error using the cubic Hermite element is about four, however, it is about 11 for the quintic element. The convergence analysis demonstrated that a high precision finite element method is able to solve the stability problem accurately within only a few elements. The present numerical technique can be easily extended to other classical flow configurations, or to complex laminar flow configurations.

ACKNOWLEDGEMENTS

The authors would like to thank Dr S. McIlwain for reviewing this paper and for providing constructive comments.

REFERENCES

1. Orszag SA. Accurate solution of the Orr–Sommerfeld stability equation. *Journal Fluid Mechanics* 1971; **50**(4):689–703.
2. Thomas LH. The stability of plane Poiseuille flow. *Physical Review* 1953; **91**:1257–1270.
3. Grosch CE, Salwen H. Hydrodynamic stability of modulated shear flow. *Physical Review Letters* 1967; **18**: 946–948.
4. Grosch CE, Salwen H. The stability of steady and time-dependent plane Poiseuille flow. *Journal of Fluid Mechanics* 1968; **34**:177–205.
5. Saraph VR, Vasudeva Rao B, Panikar JT. Stability of parallel flows by the finite element method. *International Journal for Numerical Methods in Engineering* 1979; **14**:1257–1270.
6. Fortin A, Jardak M, Gervais JJ, Pierre R. Old and new results on the two-dimensional Poiseuille flow. *Journal of Computational Physics* 1994; **115**:455–469.
7. Dongarra JJ, Straughan B, Walker DW. Chebyshev tau-QZ algorithm methods for calculating spectra of hydrodynamic stability problems. *Applied Numerical Mathematics* 1996; **22**:399–434.
8. Kirchner NP. Computational aspects of the spectral Galerkin FEM for the Orr–Sommerfeld equation. *International Journal for Numerical Methods in Fluids* 2000; **32**:119–137.
9. Lin CC. *The Theory of Hydrodynamic Stability*. Cambridge University Press: Cambridge, 1955.
10. Nachtsheim PR. An initial value method for the numerical treatment of the Orr–Sommerfeld equation for the case of plane Poiseuille flow. *NASA Technical Note, D-2414* 1964.
11. Shen SF. Calculated amplified oscillations in plane Poiseuille and Blasius flows. *Journal of Aerosol Science* 1954; **21**:62–64.
12. Mele P, Morganti M, Di Carlo A, Tatone A. Laminar to turbulent flow study by means of FEM. *Proceeding of the 2nd International Conference on Numerical Methods in Laminar and Turbulent Flow,* Venice, Italy 1981; 315–326.

